

CHEMISTRY

AN **ASIAN** JOURNAL

www.chemasianj.org

Accepted Article

Title: Nitrogen-Doped Carbon-Decorated CeO₂ Supported Pt Nanoparticles for Base-Free Aerobic Oxidation of 5-hydroxymethylfurfural

Authors: Changxuan Ke, Mengyuan Li, Guoli Fan, Lan Yang, and Feng Li

This manuscript has been accepted after peer review and appears as an Accepted Article online prior to editing, proofing, and formal publication of the final Version of Record (VoR). This work is currently citable by using the Digital Object Identifier (DOI) given below. The VoR will be published online in Early View as soon as possible and may be different to this Accepted Article as a result of editing. Readers should obtain the VoR from the journal website shown below when it is published to ensure accuracy of information. The authors are responsible for the content of this Accepted Article.

To be cited as: *Chem. Asian J.* 10.1002/asia.201800738

Link to VoR: <http://dx.doi.org/10.1002/asia.201800738>

A Journal of



A sister journal of *Angewandte Chemie*
and *Chemistry – A European Journal*

WILEY-VCH

Nitrogen-Doped Carbon-Decorated CeO₂ Supported Pt Nanoparticles for Base-Free Aerobic Oxidation of 5-hydroxymethylfurfural

Changxuan Ke⁺, Mengyuan Li⁺, Guoli Fan^{*}, Lan Yang and Feng Li^{*}

Abstract: Currently, the base-free aerobic oxidation of biomass-derived 5-hydroxymethylfurfural (HMF) to produce 2,5-furandicarboxylic acid (FDCA) is attracting intensive interest due to its prospects for the green, sustainable and promising production of bio-based aromatic polymers. In this work, we developed a new nitrogen-doped carbon-decorated CeO₂ (NC-CeO₂) supported Pt catalyst for aerobic oxidation of HMF in water without addition of any homogeneous base. It was demonstrated that small-sized Pt particles could be well dispersed on the surface of the hybrid NC-CeO₂ support, and the activity of supported Pt catalysts depended strongly on surface structure and property of catalysts. As-fabricated Pt/NC-CeO₂

catalyst with abundant surface defects, enhanced basicity, and favourable electron-deficient metallic Pt species enabled an almost 100 % yield of FDCA in water using molecular oxygen of 0.4 MPa at 110 °C for 8 h without the addition of any homogeneous base additive, indicative of an exceptional catalytic performance. What's more, the present Pt/NC-CeO₂ catalyst also possessed good stability and reusability, owing to strong metal-support interactions. Understanding the role of surface structural defects and basicity of hybrid NC-CeO₂ support provides a basis for rationally designing high performing yet stable supported metal catalysts applied practically in various transformations of biomass-derived compounds.

Introduction

Nowadays, the emission of greenhouse gases caused by using non-renewable energy sources such as fossil fuels is becoming increasingly serious.^[1] Currently, biomass resource is the most promising alternative to fossil fuels and petrochemicals. However, the application of biomass has led to some controversy, such as the production of bioethanol derived from corn and sugar cane.^[2] For these reasons, today's biomass research is moving towards non-edible raw materials, such as lignocelluloses.^[3] Especially, bio-based furfural derivatives with several functional groups become important platform compounds to produce chemicals.^[4] It is particularly noteworthy that 2,5-furan dicarboxylic acid (FDCA) obtained by the oxidation of cellulose-derived 5-hydroxymethylfurfural (HMF) can be used as a synthetic biomass-based polymer monomer replacing traditional fossil-derived terephthalic acid in the economically viable production of value-added polyethylene terephthalate, polybutylene terephthalate and other polymers,^[5] as well as a building block for constructing metal-organic framework materials, which can solve harmful effects of terephthalic acid on living organisms due to its bioaccumulation.

In the past decade, selective oxidation of HMF to produce FDCA has experienced from the initial use of stoichiometric oxidants to the current metal-catalyzed aerobic oxidation processes.^[6] For the latter, noble metals (e.g. Au,^[7-12] Pt,^[11,13-16] Au-Cu,^[9] Au-Pd,^[17-19] Ru^[20]) are especially active at appropriate oxygen pressures and reaction temperatures. In most cases, however, homogeneous base additives (e.g. Na₂CO₃ or NaOH) still are required to promote this tandem reaction, especially the hydroxyl group oxidation. So far, the pathways available for the industrial production of FDCA through catalytic oxidation processes have not been applied. The main limiting factor is that the catalyst stability and processing efficiency still are not very satisfactory. Moreover, excess amounts of base additives added can cause a strong corrosion to the equipment and simultaneously lead to serious environmental pollution. To improve the catalytic performances of supported catalysts, numerous researchers have focused on the study of different catalyst supports (e.g. carbon nanotubes,^[14,21] layered double hydroxides (LDHs),^[10,12,20-23] zinc hydroxycarbonate,^[19] carbon materials,^[15,17,24,25] metal oxides^[7-9,20,25]). Commonly, a strongly alkaline aqueous medium or adding extra homogeneous base is required to achieve high yields of FDCA.^[8,26] Meanwhile, due to the formation of acidic FDCA in the absence of homogeneous base in reaction media, the easy leaching of active metal components can result in a rapid deactivation in the case of LDHs-supported catalysts.^[21,23] Although covalent triazine frameworks supported Ru clusters exhibited good stability in the above reaction,^[24,27] low FDCA yields (< 90%) were obtained. Therefore, designing new stable support materials applied in the catalytic base-free aerobic oxidation of HMF is greatly desirable in terms of highly efficient production and environmental protection.

As one of the most widely applied metal oxides, ceria has been used as the wonderful catalyst support and actual catalyst, because of its unique physicochemical properties including

C. Ke⁺, M. Li⁺, Dr. G. Fan, Prof. L. Yang, Prof. F. Li
State Key Laboratory of Chemical Resource Engineering, Beijing
Advanced Innovation Center for Soft Matter Science and Engineering,
Beijing University of Chemical Technology, P. O. BOX 98, Beijing 100029,
P. R. China.

E-mail: fangl@mail.buct.edu.cn; lifeng@mail.buct.edu.cn
Fax: +8610-64425385; Tel.: +8610-64451226

[⁺] These authors contribute equally to this work.

Supporting information for this article is available on the WWW under
<http://dx.doi.org/10.1016/j.apcata.xxxx>.

FULL PAPER

tunable acid-base property, good thermal/chemical stability, favorable structural defects, and storage capacity of oxygen.^[28,29] On the other side, it is generally accepted that for supported catalyst systems, suitable metal-support interactions can significantly heighten their catalytic performances.^[30] Accordingly, manipulating surface structure and property of catalyst supports is of vital importance. Recently, nitrogen-doped carbon (NC) materials, typically graphitic carbon nitride (*g*-C₃N₄) possessing the graphite-like sp²-bonded C–N structure,^[31] are attracting considerable attention in the field of heterogeneous catalysis,^[32–35] due to their unique structures and properties.^[36,37] Specially, the electron-rich character of nitrogen atoms in the structure of NC frameworks can induce the generation of surface basic sites,^[38–40] while the catalyst stability can be largely improved by the interacting of active species with the NC support.

In this contribution, we reported a new nitrogen-doped carbon-decorated CeO₂ (NC-CeO₂) supported Pt nanoparticles (NPs) and investigated its catalytic performance in the base-free oxidation of HMF in water using molecular oxygen. It was demonstrated that as-fabricated Pt/NC-CeO₂ catalyst afforded an exceptionally high FDCA yield of 100% under mild reaction conditions (*i.e.* oxygen of 0.4 MPa, 110 °C, 8 h). The study on the structure–performance correlation of catalysts revealed that both enhanced surface basicity originating from NC component and abundant structural defects of CeO₂ component (*e.g.* oxygen vacancies and Ce³⁺ species), as well as favorable electron-deficient Pt⁰ species, played crucial roles in activating reactants and forming FDCA product.

Results and Discussion

Structural characterization of supported Pt samples

Figure 1 shows the XRD patterns of three different supported Pt samples. One can clearly see the coexistence of *g*-C₃N₄ and metallic Pt⁰ phases in the Pt/C₃N₄ sample, as evidenced by the appearance of the characteristic (002) diffraction for *g*-C₃N₄ phase and (111), (200), (220) and (311) diffractions for metallic Pt⁰ phase. The XRD patterns of two CeO₂-containing Pt samples present a series of characteristic diffractions of cube fluorite-type CeO₂ (JCPDS No.43-1002), and no diffractions assignable to metallic Pt phase can be observed, mirroring the highly dispersive

character of Pt species on the surface. For Pt/NC-CeO₂ sample, it is difficult to find the characteristic (002) plane of crystalline *g*-C₃N₄ phase, probably due to the formation of a relatively small amount of amorphous NC uniformly dispersing on the surface CeO₂. Elemental analysis by ICP-AES reveals a Pt loading of about 0.6 wt% on different samples (Table 1), indicating that most of the active metal has been loaded on the surface of different supports.

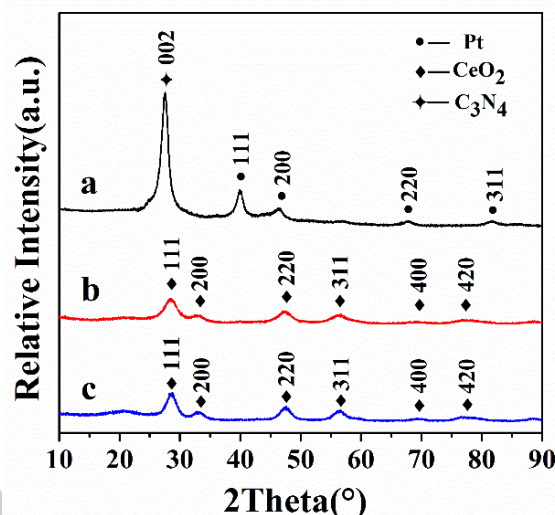


Figure 1 XRD patterns of Pt/C₃N₄ (a), Pt/CeO₂ (b), Pt/NC-CeO₂ (c) samples.

Figure 2 depicts HRTEM images of supported Pt samples. It is clearly noted that a few irregular black Pt nanoparticles (NPs) of about 4.5 nm in diameter disperse on the surface of the sheet-like *g*-C₃N₄ support in the Pt/C₃N₄ sample. For Pt/CeO₂, it is observed that the characteristic (111) planes for metallic Pt⁰ and CeO₂ phases can be preferentially exposed on the surface, respectively. In the case of Pt/NC-CeO₂ sample, besides Pt⁰ NPs, crystalline CeO₂ NPs are uniformly distributed over the surface. Noticeably, a few interspersed amorphous NC thin layers are randomly distributed over the surface. The average size of Pt NPs on Pt/NC-CeO₂ (3.1 nm) is slightly smaller than those on Pt/CeO₂ (3.3 nm) and Pt/C₃N₄ (4.5 nm), reflecting the higher dispersion of metallic Pt particles. Obviously, in the case of Pt/NC-CeO₂, CeO₂

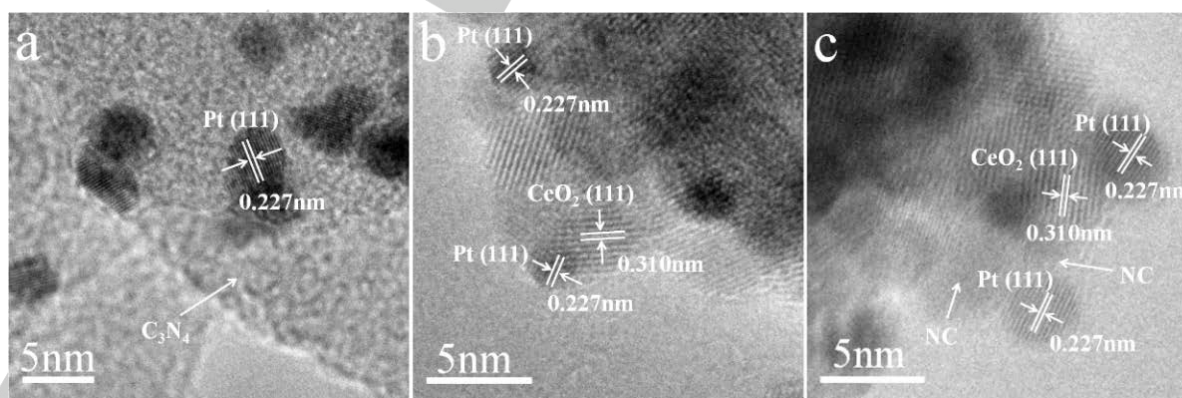


Figure 2 HRTEM images of Pt/C₃N₄ (a), Pt/CeO₂ (b) and Pt/NC-CeO₂ (c) samples

FULL PAPER

and NC components can be integrated together into the highly hybridized structure, thus being beneficial to the homogeneous dispersion of Pt NPs. As shown in Figure 3, HAADF-STEM image and EDX element mappings of the representative Pt/NC-CeO₂ sample present the special distributions of C, N, O, Pt and Ce elements on the surface. Obviously, the distributions of surface C, N, O and Ce elements based on EDX element mappings are well consistent with the overall shape of the tested region of the sample, further mirroring that CeO₂ and NC are evenly distributed throughout the sample. ICP-AES results show that Pt content is 0.6 wt%, and Ce content is 79.1 wt%, so the mass ratio of CeO₂ in the Pt/CN-CeO₂ catalyst is about 98.2%.

In addition, the adsorption-desorption isotherms of Pt/CeO₂ and Pt/NC-CeO₂ samples are characteristic of type IV possessing a H2-type hysteresis loop (Figure S1), indicative of the typical mesoporous structure with the interconnected pore system. Meanwhile, Pt/C₃N₄ sample shows the isotherms of type IV with the H1-type hysteresis loop at the P/P₀ range from 0.75 to 1.0, indicative of a mesoporous structure having cylindrical channels. As listed in Table 1, among three Pt-samples, Pt/CeO₂ sample has a highest specific surface area, because the surface of CeO₂ is partially covered by the NC component, thus leading to the blocking of some mesopores.

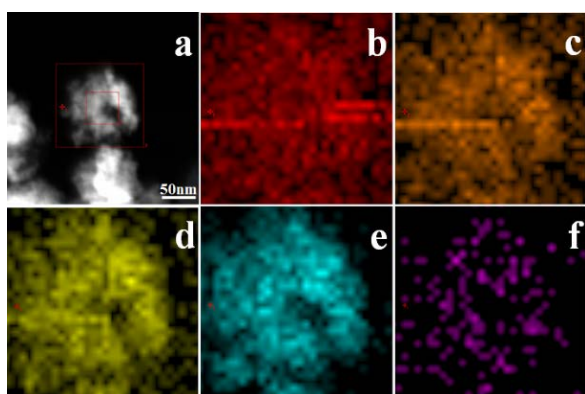


Figure 3 HAADF-STEM image (a) and EDX element mappings of C-k (b), N-k (c), O-k (d), Ce-L (e) and Pt-L (f) in the Pt/NC-CeO₂ sample.

Surface structural property of supported Pt samples

CO₂-TPD experiments were performed to obtain surface basicity of samples. As shown in Figure 4, Pt/CeO₂ sample shows a small desorption at about 100 °C and a large and broad desorption in the range of 150-550 °C, which are associated with weak base (WB) sites and medium-strength Lewis base (MLB) sites, respectively.^[41] In the case of Pt/C₃N₄-CeO₂, in addition to those related to WB and MLB sites, a small desorption appears at the higher temperature of about 630 °C, which can be assignable to strong Lewis base (SLB) sites.^[42] Such newly-developed SLB sites on the Pt/NC-CeO₂ can result from the electron-rich nitrogen atoms of NC component.^[12,43] Meanwhile, the density of total basic sites (0.2795 mmol/g) for Pt/CeO₂ is larger than that for Pt/NC-CeO₂ (0.1803 mmol/g). The reduced total basic sites on the Pt/NC-CeO₂ is mainly due to the partial overlapping of surface CeO₂ with NC component in the hybrid NC-CeO₂ support, thus inhibiting the exposure of MLB sites. Based on the above CO₂-

TPD results, it is demonstrated that the introduction of NC component can strengthen surface basicity of Pt/NC-CeO₂, despite the reduced total base sites.

To elucidate the surface electronic structure of Pt species, supported Pt samples were characterized by XPS (Figure 5). In the fine Pt 4f spectra of samples, there are two Pt 4f_{7/2} and 4f_{5/2} spin-orbit components at about 70.6 and 73.9 eV, respectively, indicating the presence of metallic Pt⁰ species.^[44] Interestingly, compared with those on the Pt/C₃N₄, the binding energy of Pt⁰ species on Pt/NC-CeO₂ and Pt/CeO₂ samples present a large positive shift of ca. 1.0 eV. Such a positive shift is an indication of the strong interactions between Pt species and CeO₂-containing supports, thereby resulting in the electron transfer from Pt⁰ to the support and thus the generation of electron-deficient metallic Pt species. In each case, another two small components at about 71.6 eV and 75.5 eV in Pt samples are assigned to cationic Pt²⁺ species. As shown in Table 1, compared with that on the Pt/C₃N₄, the higher relative proportions of surface Pt²⁺ species on Pt/NC-CeO₂ and Pt/CeO₂ samples suggest that Pt atoms more easily interact with surface sites on the CeO₂ component, thereby generating more Pt²⁺ species. The electron-deficient Pt⁰ species are expected to enhance the catalytic performance via the easy activation of the oxygen molecule in the HMF oxidation.

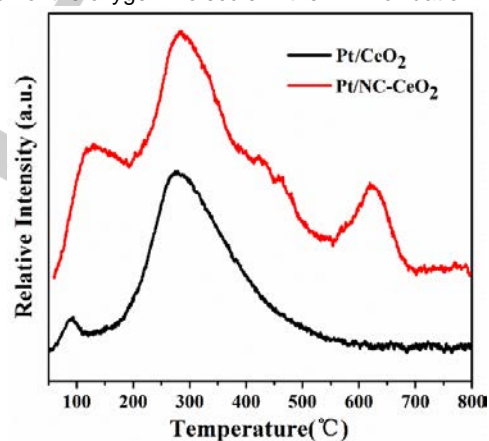


Figure 4 CO₂-TPD profiles of Pt/CeO₂ (a), Pt/NC-CeO₂ (b) and Pt/C₃N₄ (c) samples.

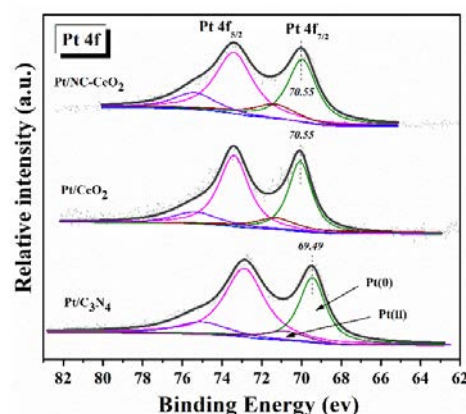


Figure 5 Pt 4f XPS of different Pt-based samples.

FULL PAPER

Figure 6 shows the Ce 3d spectra of CeO₂-containing samples. There are two types of V and U signals for Ce species related to 3d_{5/2} and 3d_{3/2} spin-orbit components, which may be finely fitted into four pairs of doublets.^[45] Among them, Ce⁴⁺ species mainly correspond to three (V₀, U₀), (V^{''}, U^{''}) and (V^{'''}, U^{'''}) doublets with different unoccupied 4f⁰ configurations,^[46] while Ce³⁺ species with 4f¹ states contribute to another pair of doubles (V', U').^[47] Interestingly, it is noted from Table 1 that surface Ce³⁺/(Ce³⁺+Ce⁴⁺) atomic ratio on the Pt/CeO₂ (0.26) is larger than that on the Pt/NC-CeO₂ (0.20), indicating that Pt/CeO₂ possesses more surface Ce³⁺ species. The presence of Ce³⁺ species is associated with the formation of surface oxygen vacancies (O_v). In comparison to Pt/CeO₂, the reduced amount of surface defects

(including Ce³⁺ species and oxygen vacancies) on the Pt/NC-CeO₂ should be attributable to the surface covering of NC component. Further, the fine O 1s spectra are deconvoluted into two components: one at 529.3 eV (O_I) and another at 531.2 eV (O_{II}), which are correlated with the lattice oxygen and defective oxide (*i.e.* oxygen vacancies) or surface hydroxyl groups.^[48] Especially, Pt/CeO₂ presents a higher surface O_{II}/(O_I+O_{II}) atomic ratio (0.61) than Pt/NC-CeO₂ (0.43), suggestive of the formation of more oxygen vacancies. The result is in good agreement with the Ce 3d XPS results. As a result, it is speculated that in the present Pt/CeO₂ and Pt/NC-CeO₂ samples, Pt species may strongly interact with surface defects of CeO₂ or NC-CeO₂, thus giving rise to electron-deficient Pt⁰ species.

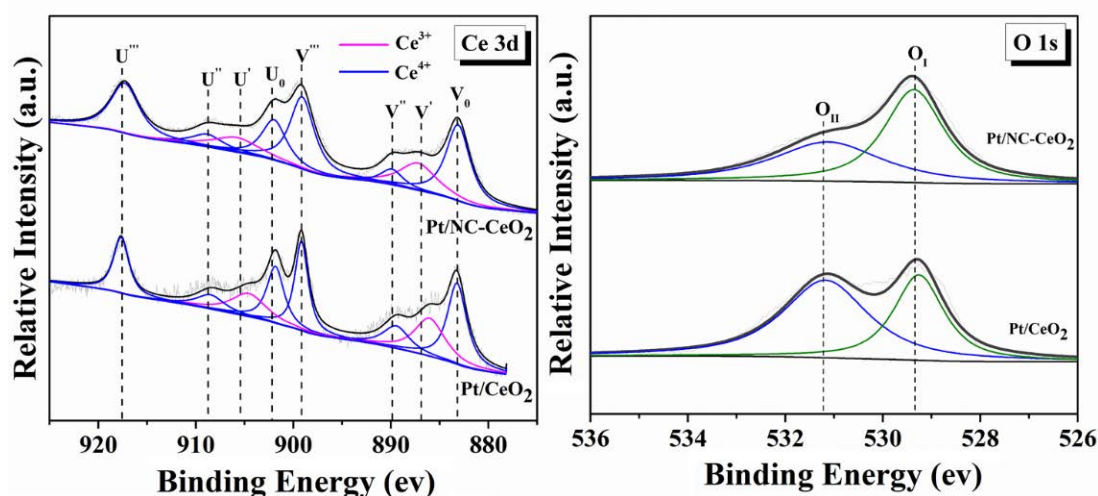


Figure 6 Ce 3d and O 1s XPS of Pt/CeO₂ and Pt/NC-CeO₂ samples.

Table 1 The compositional and structural properties of samples.

Samples	Content (wt.%)			S _{BET} ^[c] (m ² /g)	V _p ^[d] (cm ³ /g)	D _p ^[e] (nm)	Pt ⁰ /(Pt ⁰ + Pt ²⁺) ratio ^[f]	Ce ³⁺ /(Ce ³⁺ + Ce ⁴⁺) ratio ^[f]	O _{II} /(O _I + O _{II}) ratio ^[f]
	Pt ^[a]	C ^[b]	N ^[b]						
Pt/C ₃ N ₄	0.60	--	--	13.8	0.085	24.6	0.82	--	--
Pt/CeO ₂	0.61	0	0	207.7	0.167	3.9	0.74	0.26	0.61
Pt/NC-CeO ₂	0.60	7.4	2.0	153.5	0.125	3.5	0.70	0.20	0.43

[a] Determined by ICP-AES; [b] Determined by elemental microanalysis; [c] Specific surface area calculated by the BET method; [d] Pore volume; [e] Mean pore dimetersize; [f] Determined by XPS analysis.

Raman analysis of CeO₂-containing samples was conducted to identify the arrangement of metal-oxygen bonds in samples (Figure S2). Clearly, pristine CeO₂ show a strong Raman peak at 460 cm⁻¹ and two weak peaks at 600 and 1180 cm⁻¹, which are correlated with fluorite structure of CeO₂ and the lattice distortion, respectively.^[49] In this context, Ce³⁺ ions in the structure of CeO₂ may induce the shift of neighboring oxygen atoms towards Ce³⁺, thus leading to the oxygen distortion. Accordingly, the lattice distortion of CeO₂ implies the formation of oxygen vacancies and Ce³⁺ species. When Pt species are loaded on the surface of CeO₂ or NC-CeO₂, the Raman peak related to the lattice distortion is obviously reduced, probably due to the interactions between Pt species and surface defects of supports. Meanwhile, there are two weak Raman peaks at about 567 and 655 cm⁻¹ in the cases of Pt/CeO₂ and Pt/NC-CeO₂, respectively, which are correlated with the vibrations of Pt-O-Ce bond and Pt-O bond.^[49] The above

Raman results further confirm the strong metal-support interactions and the presence of surface defects in the cases of CeO₂-containing supported Pt samples.

To obtain the information on the surface electronic property of C and N species, C 1s and N 1s spectra of Pt/NC-CeO₂ sample were analyzed (Figure 7). In the fine C 1s spectrum, three contributions are assignable to three different carbon-containing functional groups: carbon with sp² hybridized structure (284.6 eV), C=N or C-OH group (286.5 eV), and C-N or carboxyl group (288.5 eV).^[50] At the same time, the broad N 1s spectrum is fitted into four components, which are associated with pyridinic N (399.2 eV), pyrrolic N (399.7 eV), graphitic N (400.8 eV), and oxidized N (402.5 eV), respectively.^[51] This result further illustrates the formation of NC component in the Pt/NC-CeO₂ sample. Accordingly, as-formed surface electron-rich N sites in the NC component, especially, pyridine-type nitrogen species,^[12] may

For internal use, please do not delete. Submitted_Manuscript

FULL PAPER

generate new SLB sites, which can promote the selective oxidation of HMF. Moreover, it is believed that pyrrole-type nitrogen species are beneficial to the dispersion of active

metals,^[52] thus governing the catalytic performance of the present Pt/NC-CeO₂ catalyst to some extent.

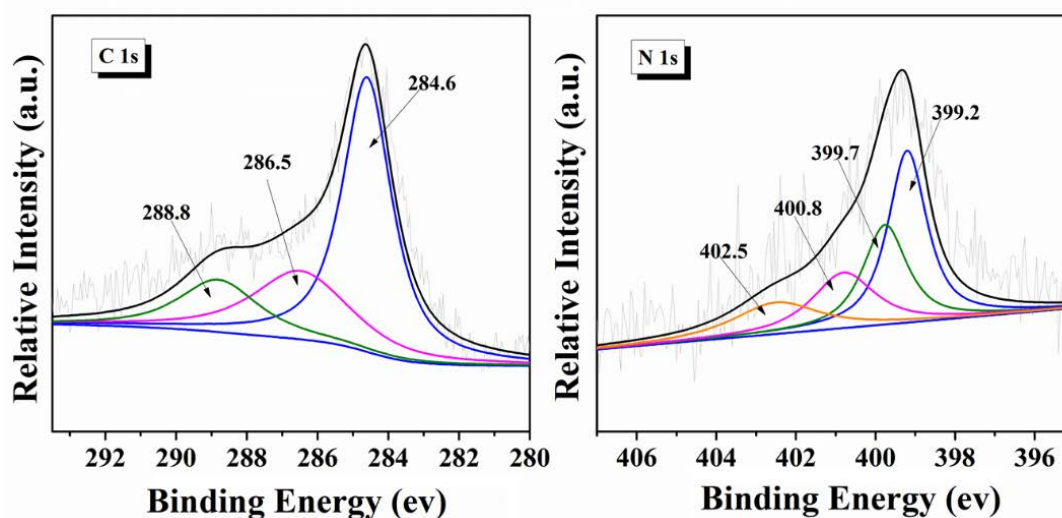


Figure 7 C 1s XPS (a), N 1s XPS (b) of Pt/NC-CeO₂ sample.

Catalytic HMF oxidation over supported Pt catalysts

As it is known, during the HMF oxidation using molecular oxygen, HMF can be first oxidized into 2,5-diformylfuran (DFF) or 5-hydroxymethyl-2-furancarboxylic acid (HMFCFA) intermediate. Subsequently, DFF or HMFCFA can be further converted into 5-formyl-2-furancarboxylic acid (FFCA). At last, FDCA is produced by a deep oxidation of FFCA.

The aerobic HMF oxidation in water was conducted over different Pt-based catalysts using molecular oxygen (0.4 MPa) within 4 h at 150 °C without the addition of any homogeneous base, and the reaction results are summarized in Table 2. Noticeably, pristine CeO₂ support in the absence of active Pt species only affords a very low HMF conversion of ~0.3 % (Entry 1), indicating that it is not active for the HMF oxidation. Pt/C₃N₄ catalyst exhibits a high HMF conversion of 71.9 %, along with a

Table 2 Catalytic performance for base-free oxidation of HMF over different catalysts ^[a]

Entry	Catalysts	HMF/Pt molar ratio	Conv. (%)	Selectivity (%)			
				FDCA	FFCA	DFF	HMFCFA
1	CeO ₂	--	0.3	7.7	22.8	69.5	0
2	Pt/C ₃ N ₄	163	71.9	18.1	43.4	38.2	0.3
3	Pt/CeO ₂	160	97.8	71.0	24.9	4.1	0
4	Pt/NC-CeO ₂	163	100	99.9	0.1	0	0
5	Pt/CeO ₂ ^[b]	163	98.6	85.2	13.6	1.2	0
6	Pt/C ₃ N ₄ + CeO ₂ ^[c]	326	42.9	20.3	45.7	33.6	0.4
7	5 wt% Pt/C	19	55.6	65.1	22.4	12.3	0.2

[a] Reaction conditions: catalyst, 0.1g; HMF, 0.5 mmol; O₂ pressure, 0.4 MPa; reaction time, 4 h; reaction temperature, 150 °C. [b] CeO₂ was reduced at 500 °C for 2 h in 10% (v/v) H₂/Ar atmosphere. [c] 0.05 g Pt/C₃N₄ and 0.05 g CeO₂

low FDCA selectivity of 18.1 % (Entry 2), while Pt/CeO₂ catalyst gives higher HMF conversion of 97.8 % and FDCA selectivity of 71.0 % (Entry 3). In the above cases, DFF and FFCA can be formed as main oxidation intermediates during the oxidation of HMF. It demonstrates that the employment of Pt/C₃N₄ and Pt/CeO₂ as catalysts leads to the formation of incomplete

oxidation products within 4 h. The HMF conversion and FDCA selectivity over commercial Pt/C catalyst with high Pt loading (5 wt%) are only 55.6 % and 65.1 %, respectively, far from satisfactory. Notably, when Pt/NC-CeO₂ is used as the catalyst, the conversion and the FDCA selectivity can reach 100 % and 99.9 % after a reaction time of 4 h even under a high HMF/Pt

For internal use, please do not delete. Submitted_Manuscript

FULL PAPER

atomic ratio of 163 (Entry 4), respectively, indicative of an exceptional catalytic performance of Pt/NC-CeO₂ catalyst. Therefore, hybrid NC-CeO₂ support is apparently superior to the sole C₃N₄ or CeO₂ support in the aerobic oxidation of HMF into FDCA. And, it is interestingly noted that compared to untreated CeO₂ support, H₂-treated CeO₂ support for loading active Pt species promotes the formation of FDCA product, along with a higher FDCA selectivity of 85.2 % (Entry 5), despite a slightly increased conversion of HMF. The catalytic performance over a physical mixture of Pt/C₃N₄ and CeO₂ (Pt/C₃N₄ + CeO₂) was also studied. For the purpose of facilitating the comparison, the catalyst loading is maintained at 0.1 g. it can be seen that the molar ratio of HMF/Pt of Pt/C₃N₄ + CeO₂ catalyst mixture is about twice as that of Pt/NC-CeO₂ or Pt/C₃N₄. The yield of FDCA over Pt/C₃N₄ + CeO₂ catalyst mixture (8.7 %) is a little higher than half that of Pt/C₃N₄ (13.0%) resulting from the addition CeO₂ with abundant surface base sites, but far lower than half that of Pt/NC-CeO₂ (~50%), probably attribute to the lack of electron-deficient Pt⁰ species. In addition, when we increase the amount of HMF from 0.5 to 1, 1.5, and 2 mmol, a nearly 100% FDCA yield can be achieved over Pt/NC-CeO₂ catalyst after reacting for 7, 11, and 15 h under the similar reaction conditions, respectively, further reflecting the excellent catalytic performance of the Pt/NC-CeO₂ catalyst. However, due to the low solubility of FDCA, when the amount of HMF higher than 0.5 mmol, FDCA precipitation can be formed under our experimental condition, causing problems for the separation of the catalyst. Hence, in view of the solubility of FDCA at room temperature, the concentration of HMF was set at 0.5 mmol in the following tests.^[53] Furthermore, after one reaction, ICP-AES result indicates that Ce concentration in the reaction filtrate is only about 8.2 ppm, i.e., the molar ratio of FDCA /Ce is about 2.1 × 10⁵, hence the influence of the formation of salt of FDCA on the catalytic performance can be neglected. The above results illustrate that the surface area of catalysts is not a crucial factor in improving the catalytic performances, because Pt/NC-CeO₂ has a lower surface area than Pt/CeO₂ (Table 1). Moreover, the leaching of Pt/NC-CeO₂ catalyst was investigated under the same reaction conditions. First, the catalyst was added into the water without reactants at 150 °C with O₂ (0.4 MPa). After 4 h, the catalyst was filtered and HMF was added into the solution to carry out another oxidation reaction. One can note that no conversion

of HMF can be detected, indicative of no Pt leaching in the present Pt/NC-CeO₂.

To obtain the information on the reaction pathways over the Pt/NC-CeO₂ catalyst, we monitored the change in the HMF conversion and product selectivities with the reaction time at a lower reaction temperature of 110 °C. As shown in Figure 8a, the reaction time can significantly influence the distributions of products. Noticeably, both the HMF conversion and the selectivity to FDCA gradually increase with increasing of reaction time. Within the initial 30 min, HMF conversion rapidly reaches as high as 46.8 %, along with the selectivity of DFF, FFCA and FDCA accumulating to 48.7, 41.2 and 9.9 %, respectively. DFF intermediate diminishes gradually with the prolonged reaction time, while the selectivity to FFCA slowly increases in the initial 1 h and starts to decline gradually with the further increase in the reaction time. Finally, HMF completely converts after a reaction time of 5 h. Whereas an almost 100 % yield of FDCA is achieved after a reaction time of 8 h. It is clearly mentioned that no any aldehyde group oxidized HMFOA intermediate can be detected at initial reaction period. Therefore, FFCA should be produced via DFF intermediate, like Ru-catalyzed HMF oxidation.^[54] Meanwhile, to elucidate the catalytic ability of Pt-based catalysts for the hydroxyl group oxidation, the oxidation of furfuryl alcohol (FOL) as the reaction substrate was further carried out over different supported Pt catalysts (Table 3). Notably, the FOL oxidation over the Pt/NC-CeO₂ is much faster than those over Pt/C₃N₄ and Pt/CeO₂, thereby giving rise to both the high conversion of 99.9 % and the high furoic acid selectivity of 98.6 %. It means that like HMF, FOL also can be first oxidized to furaldehyde via the alcoholic hydroxyl group oxidation and then to furoic acid in the present cases of Pt-based catalysts.

Table 3 Catalytic performance for base-free oxidation of FOL over different catalysts.^[a]

Entry	Catalysts	Conv. (%)	Selectivity (%)	
			Furaldehyde	2-furoic acid
1	Pt/C ₃ N ₄	56.2	76.1	23.9
2	Pt/CeO ₂	83.6	23.8	76.2
3	Pt/NC-CeO ₂	99.9	1.4	98.6

[a] Reaction conditions: catalyst, 0.1 g; FOL, 0.5 mmol; O₂ pressure, 0.4 MPa; reaction time, 4 h; reaction temperature, 150 °C; CH₃CN: water (v/v = 50/50), 40 mL.

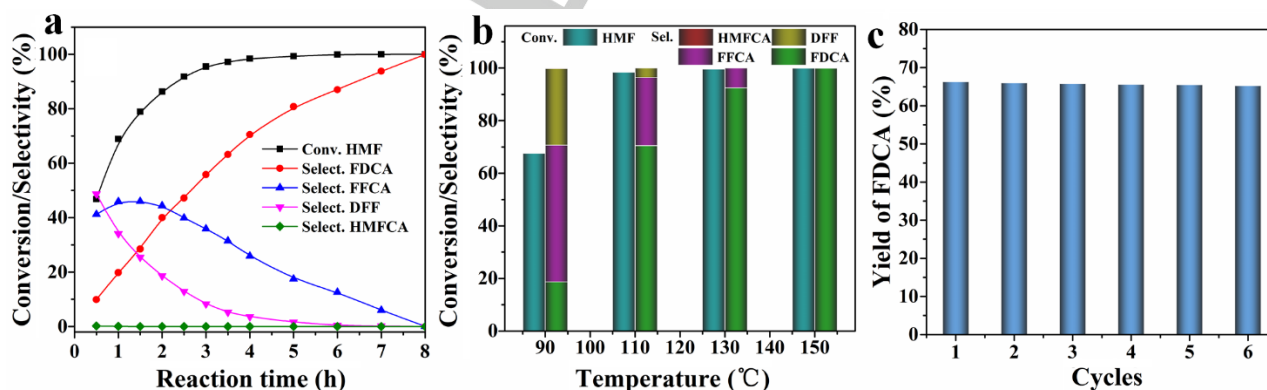


Figure 8 Effects of reaction time (a), reaction temperature (b) and reaction cycles (c) on HMF oxidation over the Pt/NC-CeO₂ sample. Reaction conditions: (a) reaction temperature, 110 °C; (b) reaction time, 4 h; (c) reaction temperature, 150 °C and reaction time, 1 h.

FULL PAPER

Based on the product distributions, HMF can be rapidly oxidized to produce DFF intermediate over the Pt/NC-CeO₂ catalyst, which is further oxidized to FFCA and then FDCA. Throughout the reaction, the selectivity of FDCA gradually increases, indicating that this product is quite stable under the present reaction conditions. Conversely, previous results revealed that the oxidation with base additive over Au/TiO₂, Au/CeO₂, and Au/LDH could first proceed by the oxidation of aldehyde group in HMF.^[7,8,20] It suggests that support structure of the present Pt/NC-CeO₂ catalyst should have a preferential effect on the activation and oxidation of the hydroxymethyl group in HMF, thus leading to the effective oxidation from alcohol to aldehyde and further carboxylic acid products. More importantly, despite different reaction conditions, the turnover number (TON) for FDCA formed over the

Pt/NC-CeO₂ at 110 °C after 8 h reaches as high as 163, which is higher than those over other metal-based catalysts previously reported in the absence of the additional homogeneous base (Table S1). In addition, contrast experiments were performed to address the necessity of a base under high dilution conditions in our case. As listed in Table 4, though with same HMF/Pt molar ratio (163), when NaHCO₃ was added, the yield of FDCA increased from 13.6 % to 43.2%. Similarly, after addition of support with abundant base sites (CeO₂, C₃N₄), the yield of FDCA increased slightly under the similar reaction condition. The above results indicate that base sites in our catalyst indeed has a positive effect on the yield of FDCA and a base is necessary even under high dilute conditions.

Table 4 Catalytic performance for oxidation of HMF over different catalysts^[a]

Entry	Catalysts	HMF/Pt molar ratio	Conv. (%)	Selectivity (%)			
				FDCA	FFCA	DFF	HMFCa
1	Pt/NC-CeO ₂	163	68.9	19.8	45.9	34.1	0.1
2	Pt/NC-CeO ₂ + 0.1 g NaHCO ₃	163	89.7	48.2	35.3	16.3	0.2
3	Pt/NC-CeO ₂ + 0.1 g CeO ₂	163	74.2	24.6	46.2	29.1	0.1
4	Pt/NC-CeO ₂ + 0.1 g C ₃ N ₄	163	71.8	22.1	46.8	31.1	0

[a] Reaction conditions: catalyst, 0.1 g; HMF, 0.5 mmol; O₂ pressure, 0.4 MPa; reaction time, 1 h; reaction temperature, 110 °C.

Further, the effect of the reaction temperature on the HMF oxidation catalyst was investigated over the Pt/NC-CeO₂ (Figure 8b). It is obvious that the HMF conversion and the FDCA selectivity are remarkably improved as the reaction temperature is elevated from 90 to 150 °C. When the reaction temperature is raised to 150 °C, an almost 100 % yield of FDCA is achieved with the complete conversion of DFF and FFCA intermediates. It illustrates that high reaction temperatures can promote the oxidations of alcoholic hydroxyl and carbonyl groups in reactants and intermediates to achieve desired FDCA product.

In addition, we investigated the recyclability of Pt/NC-CeO₂ catalyst (Figure 8c). After the catalyst was recovered by centrifugation and the following washing, the recovered catalyst was applied to the next reaction. After six consecutive cycles, the FDCA yield is decreased only by less than 1.0 %, indicating that the Pt/NC-CeO₂ may be recycled without a remarkable activity loss. The ICP-AES results of the reaction filtrate show a negligible leaching loss of Pt species, the N content of the spent catalyst determined by elemental analysis does not change after six runs, while the Ce leaching loss is only 1.6 wt% after the recycling test, mirroring the nearly unchanged composition of the catalyst after six runs. Moreover, the XRD patterns and TEM images reveal that the spent catalyst remains its initial structure and morphology (Figure S3), and no aggregation or growth of Pt NPs can be found. It illustrates that the present Pt/NC-CeO₂ catalyst possesses an excellent stability and recyclability, mainly attributable to strong metal-support interactions.

Mechanism of catalytic HMF oxidation

The above CO₂-TPD results reveal that Pt/NC-CeO₂ possesses a small amount of newly-developed SLB sites, despite a smaller amount of total basic sites than Pt/CeO₂. In this regard, surface strong basic sites are beneficial to the generation of negatively charged alkoxide intermediates through the interaction with the alcoholic hydroxyl group in HMF and thus the generation of β-hydride on Pt⁰ species.^[55,56] Accordingly, the surface basicity of Pt/NC-CeO₂ catalyst, especially surface strong basic sites, can play an important role in improving the oxidation of alcoholic hydroxyl group in HMF. Meanwhile, the XPS results show the presence of more surface Pt²⁺ species in the case of Pt/NC-CeO₂, besides electron-deficient Pt⁰ species. These electron-deficient Pt⁰ and cationic Pt²⁺ species may facilitate the of C-H bond dissociation and the molecular oxygen activation, like Au^{δ+} species,^[57,58] thereby benefiting for the enhanced catalytic behavior of Pt/NC-CeO₂ catalyst.

Moreover, surface Ce³⁺ species adjacent to metallic Pt⁰ species can coordinate oxygen in the alcoholic hydroxyl group or carbonyl group in HMF or DFF and FFCA, while surface oxygen vacancies may fix molecular oxygen and facilitate the decomposition of O-O bond in oxygen molecule, thus affording active oxygen species at the metal-support perimeter interface to accelerate the conversion of reactants. In this regard, compared with Pt/CeO₂, the enhanced catalytic activity of H₂-treated CeO₂ supported Pt one with more surface defects (Table 2, entry 5) further illustrates a promotional role of surface defects (Ce³⁺ or oxygen vacancies) in the HMF oxidation. Accordingly, surface defects of supports also should be a key factor in governing the oxidation of HMF.

In general, in the present catalytic system, the catalytic performance of supported Pt catalysts strongly depends on surface structure and property of catalysts. Correspondingly,

For internal use, please do not delete. Submitted_Manuscript

FULL PAPER

Pt/NC-CeO₂ catalyst with stronger basic sites, favorable surface oxygen vacancies/Ce³⁺ species, and unique electron-deficient Pt species shows a superior catalytic activity to Pt/CeO₂ and Pt/C₃N₄ catalysts in the HMF oxidation to produce FDCA. Nevertheless, the detailed roles of NC-CeO₂ and Pt species in the aerobic oxidation still need to be further determined by theoretical and experimental investigations accurately and systemically.

In summary, a highly efficient and stable nitrogen-doped carbon-decorated CeO₂ supported Pt-based catalyst was fabricated and applied in the oxidation of HMF to produce FDCA in water using molecular oxygen without the addition of any homogenous base. Structural characterization revealed the unique features of abundant surface defects, enhanced surface basicity, favorable electron-deficient metallic Pt species and strong metal-support interactions in the Pt/NC-CeO₂ catalyst. The developed Pt/NC-CeO₂ catalyst exhibited an exceptional catalytic efficiency with an almost 100% FDCA under mild reaction conditions, as well as an excellent stability. Moreover, the TON value for FDCA formed over the Pt/NC-CeO₂ at 110 °C after 8h could reach about 163, which was higher than those over other metal-based catalysts previously reported in the absence of the additional homogeneous base. The present study provides a new approach for designing other high performing and stable supported metal catalysts based on NC-decorated metal oxide supports with adjustable active metal species and metal oxide supports applied in a variety of heterogeneous catalysis.

Experimental section

Preparation of supported Pt catalysts

Hybrid NC-CeO₂ support was synthesized by a modified solution-phase reduction-oxidation method developed by our group.^[59] First, Ce(NO₃)₃·6H₂O (0.01 mol) and melamine (0.01 mol) were dispersed and dissolved into 80 mL of deionized water to obtain solution A, while NaBH₄ (0.1 mol) was dissolved into 80 mL of deionized water to obtain solution B. Subsequently, A and B solutions were simultaneously put into a colloid mill, mixed rapidly at a 4000-rpm rotor speed for 3 min and aged at 90 °C for 24 h. The resulting precipitate was filtered, washed with deionized water, and dried at 70 °C for 12 h. At last, the resultant solid was calcined at 500 °C for 3 h under air atmosphere to form hybrid NC-CeO₂ support. Moreover, pure CeO₂ support was synthesized based on the above procedure in the absence of melamine, and pristine *g*-C₃N₄ support was synthesized by calcining melamine at 500 °C for 4 h.

Pt/NC-CeO₂ with the Pt loading of about 0.6 wt % was prepared by using NaBH₄ as reductive reagent. First, NC-CeO₂ sample (0.5 g) was put into 50 mL of aqueous solution containing H₂PtCl₆·6H₂O (0.01 g). Subsequently, 20 mL of NaBH₄ aqueous solution, where the NaBH₄/Pt molar ratio is set at 15:1, was put into the support-containing suspension and aged at 25 °C for 6h at nitrogen atmosphere. At last, the solid was dried at 70 °C under vacuum. For comparison, CeO₂ or *g*-C₃N₄ supported Pt sample also was prepared according to the above similar process.

Characterization

Powder X-ray diffraction (XRD) patterns of different samples were collected on a Shimadzu XRD-6000 diffractometer with Cu K α source (λ = 0.15418 nm). The Pt content in supported catalysts samples was analyzed on a Shimadzu ICPS-7500 inductively coupled plasma atomic emission spectroscopy (ICP-AES). Elemental microanalysis (Elementar Vario analyzer) was applied to analyze the contents of nitrogen and carbon elements. Low-temperature nitrogen adsorption-desorption experiments were carried out on a sorptometer apparatus (Micromeritics ASAP 2020) at 77 K. Raman spectra were collected on Princeton MontaVista Raman microscope equipped using a 532 nm excitation laser. Transmission electron microscopy (TEM) and high-resolution TEM (HRTEM) were performed using a JEOL JEM-2100 microscope. High-angle annular dark-field scanning transmission electron microscopy (HAADF-STEM) was conducted using a JEOL2010F instrument with energy-dispersive X-ray spectroscopy (EDX). X-ray photoelectron spectroscopy (XPS) was carried out on a Thermo VG ESCALAB250 spectrometer using the Al K α X-ray radiation. According to the C1s signal of 284.6 eV, the binding energies were calibrated. Temperature-programmed desorption of carbon dioxide (CO₂-TPD) was performed on Micromeritics ChemiSorb 2920. First, the sample (0.1g) was pretreated under a He flow (20 mL/min) at 100 °C for 1 h, and then exposed to a CO₂/He mixture flow (20 mL/min) at 50 °C for 1 h. Afterwards, the sample was purged using a He flow (20 mL/min) for 30 min and heated up to 800 °C at a heating rate of 10 °C /min to continuously detect carbon dioxide concentration by a thermal conductivity detector. Assuming a single carbon dioxide molecule can be adsorbed at a sole base site, the surface density of basic sites can be assessed.

Catalytic aerobic HMF oxidation

The oxidation of HMF was performed at a stainless-steel autoclave reactor. In a typical reaction, catalyst (0.1 g) and HMF (0.5 mmol) were added into 40 ml of deionized water. Then, O₂ of 0.4 MPa was purged into the reactor. At a certain reaction temperature, the reaction was initiated by magnetic stirring at a stirring speed of 900 rpm. After the oxidation, the liquid products were quantitatively analyzed by a Shimadzu LC-20A liquid chromatography with a UV detector and a HPX-87H chromatographic column (mobile phase: dilute H₂SO₄ aqueous solution of 10 mM at a flow rate of 0.6 mL/min). According to external standard curves, HMF conversion and product selectivities were obtained from three parallel experiments. In all cases, mass balances were more than 97 %.

Acknowledgments

We greatly thank the financial support from National Natural Science Foundation of China (21776017; 21521005).

Keywords: Nitrogen-doped carbon • Ceria • Surface basicity • Surface defects • Oxidation

FULL PAPER

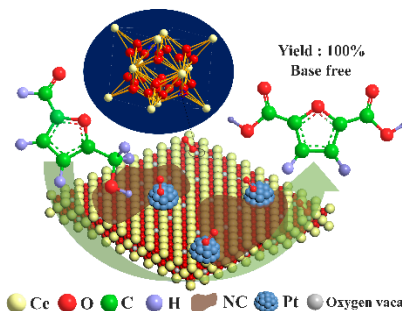
References

- [1] R.A. Sheldon. *Green Chem.* **2014**, *16*, 950–963.
- [2] M. Vohra, J. Manwar, R. Manmode, S. Padgilwar, S. Patil, J. Environ. *Chem. Eng.* **2014**, *2*, 573–584.
- [3] L. Luque, R. Westerhof, G. van Rossum, S. Oudenhoven, S. Kersten, F. Berruti, L. Rehmman, *Bioresour. Technol.* **2014**, *161*, 20–28.
- [4] M.J. Climent, A. Corma, S. Iborra. *Green Chem.* **2014**, *16*, 516–547.
- [5] J.N. Chheda, Y. Roman-Leshkov, J.A. Dumesic. *Green Chem.* **2007**, *9*, 342–350.
- [6] W.P. Dijkman, D.E. Groothuis, M.W. Fraaije. *Angew. Chem. Int. Ed.* **2014**, *53*, 6515–6518.
- [7] Y.Y. Gorbanev, S.K. Klitgaard, J.M. Woodley, C.H. Christensen, A. Riisager. *ChemSusChem* **2009**, *2*, 672–675.
- [8] O. Casanova, S. Iborra, A. Corma, *ChemSusChem* **2009**, *2*, 1138–1144.
- [9] T. Pasini, M. Piccinini, M. Blosi, R. Bonelli, S. Albonetti, N. Dimitratos, J.A. Lopez-Sanchez, M. Sankar, Q. He, C.J. Kiely, G.J. Hutchings, F. Cavani, *Green Chem.* **2011**, *13*, 2091–2099.
- [10] N.K. Gupta, S. Nishimura, A. Takagaki, K. Ebitani, *Green Chem.* **2011**, *13*, 824–827.
- [11] S.E. Davis, B.N. Zope, R.J. Davis, *Green Chem.* **2012**, *14*, 143–147.
- [12] T. Gao, T. Gao, W. Fang, Q. Cao, *Mole. Catal.* **2017**, *439*, 171–179.
- [13] S. Siankevich, G. Savoglidis, Z. Fei, G. Laurenczy, D.T.L. Alexander, N. Yan, P.J. Dyson, *J. Catal.* **2014**, *315*, 67–74.
- [14] C. Zhou, W. Deng, X. Wan, Q. Zhang, Y. Yang, Y. Wang, *ChemCatChem* **2015**, *7*, 2853–2863.
- [15] X. Han, C. Li, Y. Guo, X. Liu, Y. Zhang, Y. Wang, *Appl. Catal. A* **2016**, *526*, 1–8.
- [16] X. Han, L. Geng, Y. Guo, R. Jia, X. Liu, Y. Zhang, Y. Wang, *Green Chem.* **2016**, *18*, 1597–1604.
- [17] A. Villa, M. Schiavoni, S. Campisi, G.M. Veith, L. Prati, *ChemSusChem* **2013**, *6*, 609–612.
- [18] C.A. Antonyraj, N.T.T. Huynh, S.-K. Park, S. Shin, Y.J. Kim, S. Kim, K.-Y. Lee, J.K. Cho, *Appl. Catal. A: Gen.* **2017**, *547*, 230–236.
- [19] Z. Gui, W. Cao, S. Saravanamurugan, A. Riisager, L. Chen, Z. Qi, *ChemCatChem* **2016**, *8*, 3636–3643.
- [20] Y. Gorbanev, S. Kegnaes, A. Riisager, *Top. Catal.* **2011**, *54*, 1318–1324.
- [21] X. Wan, C. Zhou, J. Chen, W. Deng, Q. Zhang, Y. Yang, Y. Wang, *ACS Catal.* **2014**, *4*, 2175–2185.
- [22] Y. Wang, K. Yu, D. Lei, W. Si, Y. Feng, L.-L. Lou, S. Liu, *ACS Sustainable Chem. Eng.* **2016**, *4*, 4752–4761.
- [23] Z. Gao, R. Xie, G. Fan, L. Yang, F. Li, *ACS Sustainable Chem. Eng.* **2017**, *5*, 5852–5861.
- [24] G.S. Yi, S.P. Teong, Y. Zhang, *Green Chem.* **2016**, *18*, 979–983.
- [25] S.E. Davis, L.R. Houk, E.C. Tamargo, A.K. Datye, R.J. Davis, *Catal. Today* **2011**, *160*, 55–60.
- [26] H.A. Rass, N. Essayem, M. Besson, *Green Chem.* **2013**, *15*, 2240–2251.
- [27] J. Artz, R. Palkovits, *ChemSusChem* **2015**, *88*, 3832–3838.
- [28] D. Liu, W. Li, X. Feng, Y. Zhang, *Chem. Sci.* **2015**, *6*, 7015–7019.
- [29] S. Damyanova, B. Pawelec, K. Arishtirova, M.V. Martinez Huerta, J.L.G. Fierro, *Appl. Catal. A: Gen.* **2008**, *337*, 86–96.
- [30] J. Álvarez-Rodríguez, I. Rodríguez-Ramos, A. Guerrero-Ruiz, E. Gallegos-Suarez, A. Arcoya, *Chem. Eng. J.* **2012**, *204–206*, 169–178.
- [31] S.B. Yang, X.L. Feng, X.C. Wang, K. Müllen, *Angew. Chem. Int. Ed.* **2011**, *50*, 5339–5343.
- [32] Z.S. Ma, H.Y. Zhang, Z.Z. Yang, G.P. Ji, B. Yu, X.W. Liu, Z.M. Liu, *Green Chem.* **2016**, *18*, 1976–1982.
- [33] J.S. Lee, X.Q. Wang, H.M. Luo, G.A. Baker, S. Dai, *J. Am. Chem. Soc.* **2009**, *131*, 4596–4597.
- [34] R.F. Nie, H.H. Yang, H.F. Zhang, X.L. Yu, X.H. Lu, D. Zhou, Q.H. Xia, *Green Chem.* **2017**, *19*, 3126–3134.
- [35] X.H. Liu, L.J. Xu, G.Y. Xu, W.D. Jia, Y.F. Ma, Y. Zhang, *ACS Catal.* **2016**, *6*, 7611–7620.
- [36] W. Yang, T.-P. Fellinger, M. Antonietti, *J. Am. Chem. Soc.* **2011**, *133*, 206–209.
- [37] Y. Zheng, J. Liu, J. Liang, M. Jaroniec, S.Z. Qiao, *Energy Environ. Sci.* **2012**, *5*, 6717–6731.
- [38] Y. Wang, X. Wang, M. Antonietti, *Angew. Chem. Int. Ed.* **2012**, *51*, 68–89.
- [39] Z. Gao, C. Li, G. Fan, L. Yang, F. Li, *Appl. Catal. B* **2018**, *226*, 523–533.
- [40] H. Watanabe, S. Asano, S. Fujita, H. Yoshida, M. Arai, *ACS Catal.* **2015**, *5*, 2886–2894.
- [41] P. Unnikrishnan, D. Srinivas, *Ind. Eng. Chem. Res.* **2012**, *51*, 6356–6363.
- [42] Q. Hu, G. Fan, L. Yang, X. Cao, P. Zhang, B. Wang, F. Li, *Green Chem.* **2016**, *18*, 2317–2322.
- [43] J. Xu, K. Shen, B. Xue, *J. Mol. Catal. A* **2013**, *372*, 105–113.
- [44] X. Ji, X. Niu, B. Li, Q. Han, F. Yuan, F. Zaera, Y. Zhu, H. Fu, *ChemCatChem* **2014**, *6*, 3246–3253.
- [45] M. Alexandrou, R.M. Nix, *Surf. Sci.* **1994**, *321*, 47–57.
- [46] A. Fujimori, *Phys. Rev. B* **1983**, *28*, 4489–4499.
- [47] H. Chen, A. Sayari, A. Adnot, F. Larachi, *Appl. Catal. B* **2001**, *32*, 195–204.
- [48] H. Wang, Z. Qu, H. Xie, N. Maeda, L. Miao, Z. Wang, *J. Catal.* **2016**, *338*, 56–67.
- [49] J.H. Lee, Y. Ryou, X. Chan, T. Kim, D.H. Kim, *J. Phys. Chem. C* **2016**, *120*, 25870–25879.
- [50] D. Zhou, L. Yang, L. Yu, J. Kong, X. Yao, W. Liu, Z. Xua, X. Lu, *Nanoscale* **2015**, *7*, 1501–1509.
- [51] S. Chen, J. Bi, Y. Zhao, L. Yang, C. Zhang, Y. Ma, Q. Wu, X. Wang, Z. Hu, *Adv. Mater.* **2012**, *24*, 5593–5597.
- [52] W.W. Guo, H.Y. Liu, S.Q. Zhang, H.L. Han, H.Z. Liu, T. Jiang, B.X. Han, T.B. Wu, *Green Chem.* **2016**, *18*, 6222–6228.
- [53] Y.Z. Zhang, X. Guo, P. Tang, J. Xu, *J. Chem. Eng. Data* **2018**, *63*, 1316–1324.
- [54] D.K. Mishra, H.J. Lee, J. Kim, H.-S. Lee, J.K. Cho, Y.-W. Suh, Y.J. Kim, *Green Chem.* **2017**, *19*, 1619–1623.
- [55] M. Conte, H. Miyamura, S. Kobayashi, V. Chechik, *J. Am. Chem. Soc.* **2009**, *131*, 7189–7196.
- [56] H. Tsunoyama, H. Sakurai, Y. Negishi, T. Tsukuda, *J. Am. Chem. Soc.* **2005**, *127*, 9374–9375.
- [57] Z. Wu, J. Deng, Y. Liu, S. Xie, Y. Jiang, X. Zhao, J. Yang, H. Arandiyán, G. Guo, H. Dai, *J. Catal.* **2015**, *332*, 13–24.
- [58] G. Zhao, J. Huang, Z. Jiang, S. Zhang, L. Chen, Y. Lu, *Appl. Catal. B* **2013**, *140–141*, 249–257.
- [59] W. Cao, J. Kang, G. Fan, L. Yang, F. Li, *Ind. Eng. Chem. Res.* **2015**, *54*, 12795–12804

Entry for the Table of Contents

FULL PAPER

Nitrogen-doped carbon-decorated CeO₂ supported Pt-based catalyst was fabricated and applied in the oxidation of HMF to produce FDCA in water using molecular oxygen without the addition of any homogenous base. The unique features such as abundant surface defects, enhanced surface basicity, favorable electron-deficient metallic Pt species, and strong metal-support interactions endow the prepared Pt/NC-CeO₂ catalyst with exceptional catalytic efficiency and stability under mild reaction conditions



Changxuan Ke[†], Mengyuan Li[†],
Guoli Fan[†], Lan Yang and Feng Li^{*}

Page No. – Page No.

Nitrogen-Doped Carbon-Decorated
CeO₂ Supported Pt Nanoparticles
for Base-Free Aerobic Oxidation of
5-hydroxymethylfurfural